An Analysis of Airborne Measurements of Vertical Water Vapor Flux During BOMEX

B. R. BEAN, R. GILMER, R. L. GROSSMAN AND R. MCGAVIN

Wave Propagation Laboratory, NOAA/ERL, Boulder, Colo.

AND C. TRAVIS

Research Flight Facility, NOAA/ERL, Miami, Fla.

(Manuscript received 2 August 1971, in revised form 14 February 1972)

ABSTRACT

The initial analysis of the water vapor flux measurements taken onboard a NOAA DC-6 during the Barbados Oceanographic and Meteorological Experiment (BOMEX) is presented. The flux of water vapor seems to be constant in the lower subcloud layer. Day-to-day variations, as well as variations within a day, are apparent in the evaporation data. Spatial variations of evaporation also seem to be present. The average value of water vapor flux for the experimental period is ~0.5 cm day^{-1}. Spectra of the instantaneous flux reveal significant alongwind-crosswind differences. Height variation of the wavelength of maximum spectral density for crosswind runs is confirmed. The instantaneous flux is intermittent in nature. Consideration of the cross spectra and time series signatures allows some speculation upon models which may be responsible for a major portion of the water vapor transport in the lower subcloud layer during BOMEX.

1. Introduction

We report here on airborne measurements of water vapor flux made during the Barbados Oceanographic and Meteorological Experiment (BOMEX) (Holland, 1970). The aircraft used was a Research Flight Facility DC-6 instrumented with a gust probe system referenced to an inertial platform which contained high performance accelerometers. This system is capable of resolving the three components of the wind, uncontaminated by the aircraft motion (Friedman *et al.*, 1970). Water vapor density ρ_w', the prime denoting a deviation from the mean, was determined by a microwave refractometer and a thermistor (McGavin and Vetter, 1963). The vertical flux of water vapor was then calculated as

$$E=\overline{\rho_w'w'}, \tag{1}$$

where the overbar denotes either a 5- or 10-min average of data sampled at 20 times per second (Rinaldi, 1970) during level flight. At the typical airspeed of 93 m sec^{-1} this represents a flight path length of 28 or 56 km. Data were generally collected at three altitudes in the lower subcloud layer: 18 m (60 ft), 45 m (150 ft) and 152 m (500 ft).

We shall first examine E and its components, ρ_w' and w', with respect to sample length, position, height and time. We will then reexamine these data for their spectral variation. Finally, we will examine frequency distributions of ρ_w' and w' data as well as individual time series for insight into the probable mechanism(s) that may be producing vertical transport of water vapor over the BOMEX ship array.

2. Data considerations

The basic gust probe system is, by its very complexity, difficult to calibrate directly. If one, however, follows the procedure outlined by Crooks *et al.* (1968), an overall resolution of less than 1 m sec^{-1} and a wavelength response from 20 m to 14 km may be obtained. An error analysis (Appendix A) indicates that the instrumental error, $\epsilon(\rho_w'w')$, is of the order of 5% of typical BOMEX flux values and would not be expected to exceed 15% of an average flux value. As we shall see, even this latter figure is small compared to the natural variability of E.

All data were analog-recorded on magnetic tape, then passed through a 4.5-cps low-pass filter and digitized at 20 samples per second.[1] Linear trends and mean values in w and ρ_w were removed and the data were numerically low-pass filtered at 4.5 cps. The value for E was then computed as well as the cospectra, quadrature spectra and spectral coherence of $\rho_w'w'$. Individual spectra of ρ_w' and w' were also computed. The data reduction and analysis package thus allows an examination of regions in frequency space where variance is concentrated.

The basic 5-min sample was chosen from a combination of operational considerations and previous experience. Nonetheless, a number of 10-min runs were made which were then divided into 5-min segments and reanalyzed to check the choice of 5 min as a basic sample length. One would expect the 10-min samples, E_{10}^{10}, to

[1] The vertical acceleration components were digitized at 40 samples per second and integrated to 20 samples per second.

TABLE 1. Ratios of daily average water vapor vertical flux E (5-min samples).*

Date	$\frac{E(18\text{ m})}{E(45\text{ m})}$	$\frac{E(45\text{ m})}{E(152\text{ m})}$	$\frac{E(18\text{ m})}{E(152\text{ m})}$
5 May 1969	0.902	1.012	0.994
10 May 1969**	1.003	0.901	0.903
11 May 1969**	1.055	0.933	0.984
24 May 1969**	0.944	0.998	0.942
1 June 1969	0.865	1.344	1.140
Average	0.971 (26)	1.135 (27)	1.090
Standard deviation	±0.188	±0.475	±0.333

* Number of samples are given in parentheses.
** Centered on FLIP.

be consistently greater than the average of the two 5-min samples, E_5^{10}, since they would include longer wavelength contributions.

Fig. 1 compares E_{10}^{10} with E_5^{10}. One first notes the rather large variability of E_{10}^{10}. The range of 0.32 to 0.82 cm day^{-1} represents large spatial and temporal variations of E, since these data were collected flying across the BOMEX array. With the exception of the highest value, E_5^{10} differs by no more than 10% from E_{10}^{10}. This variation seems acceptable compared to the overall variations of E_{10}^{10}. Therefore, in combination with effects to be discussed in the comparison of 5- and 10-min sample length spectra, we take the 5-min sample as our basic data length.

3. Variation of average water vapor flux

We first examine the variability of E with height, having already noticed an apparent spatial variation of E (Fig. 1). Attention was restricted to those measurements taken around the Floating Laboratory and

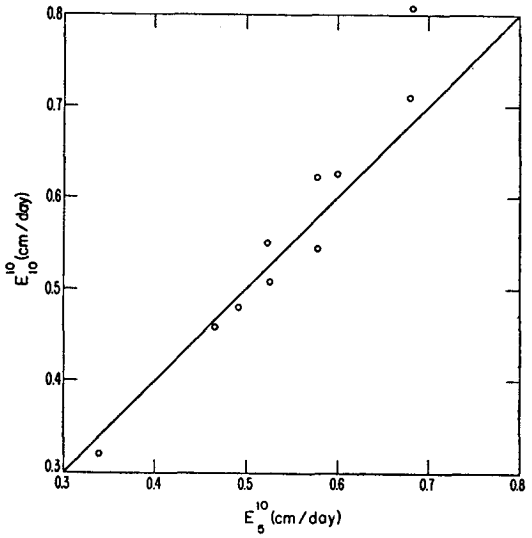

FIG. 1. Comparison of 5- and 10-min averages of water vapor flux (BOMEX 1969). Measurements were taken at 33 and 152 m at several points within the BOMEX array.

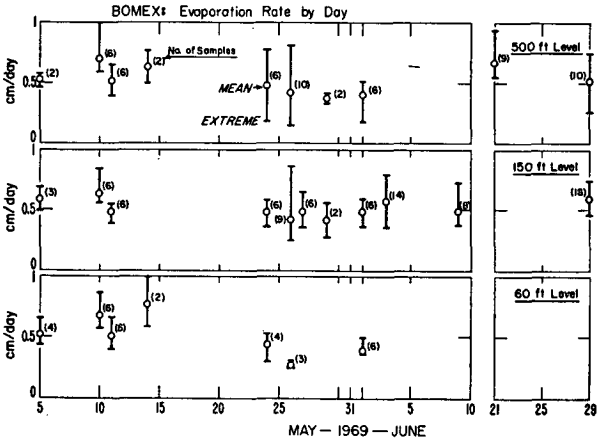

FIG. 2. Daily averages and extremes of water vapor flux taken during BOMEX. Note that day-to-day variations seem to follow at all altitudes.

Instrument Platform (FLIP) operated by Scripps Institution of Oceanography located near the center of the BOMEX array. Further, since several hours were consumed in the sampling around FLIP, values of E are averaged for each height and day. Ratios of these average values of E are presented in Table 1.

To determine whether or not the average flux is a function of altitude in the region below 150 m, a student's test of the significance for the difference in means, i.e., $E(18\text{ m})/E(45\text{ m}) - E(45\text{ m})/E(152\text{ m})$, was used. At the 5% significance level, no difference in the means could be established. Hence, we conclude that no significant difference could be found in the water vapor flux over this height range, implying a constant water vapor flux layer.

Fig. 2 presents the mean and extremes of E (both 5- and 10-min samples) as measured throughout BOMEX (5 May to 29 June 1969) and clearly shows that E is quite variable both within a day and on a day-to-day basis. Generally, the data taken prior to 1 June 1969 are centered on FLIP and represent temporal variations. After 1 June the variations within a day represent a mixed temporal and spatial variation of E within the BOMEX array. The overall averages of water vapor flux for the 181 runs analyzed for Fig. 2 are given in Table 2.

4. Spectral variability of water vapor flux

An obvious characteristic of the E spectra is the striking difference in cross- and alongwind spectra of

TABLE 2. Overall averages $\bar{E}$ of water vapor flux measurements taken during the period 5 May to 29 June.*

Height (m)	$\bar{E}$ (cm day^{-1})
18	0.517 (31)
45	0.531 (71)
152	0.509 (50)

* Number of samples are given in parentheses.

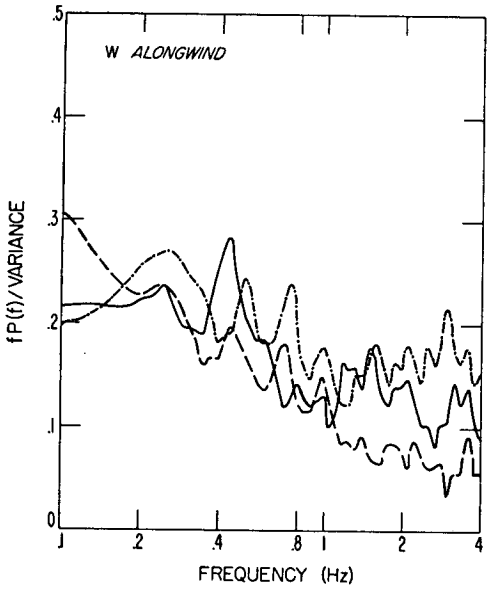

FIG. 3. Normalized frequency-weighted spectral density of vertical velocity vs altitude for three alongwind flights. The spectra are normalized to the variance. All flights were taken within an hour of one another. Altitudes: 152 m (dashed line), 45 m (solid line), 18 m (dash-dotted line).

w' and $\rho_w'w'$. Figs. 3 and 4 show spectra of vertical wind for an individual alongwind and crosswind flight. For the alongwind case we note at the very lowest frequencies that the spectral densities *increase* with height, while at the higher frequencies the spectral densities decrease with height. These trends are more pronounced in the crosswind spectra shown in Fig. 4.

The vertical variation of the spectra noticed in the individual w' spectra was so persistent that a composite spectrum, integrating the runs taken near FLIP, was

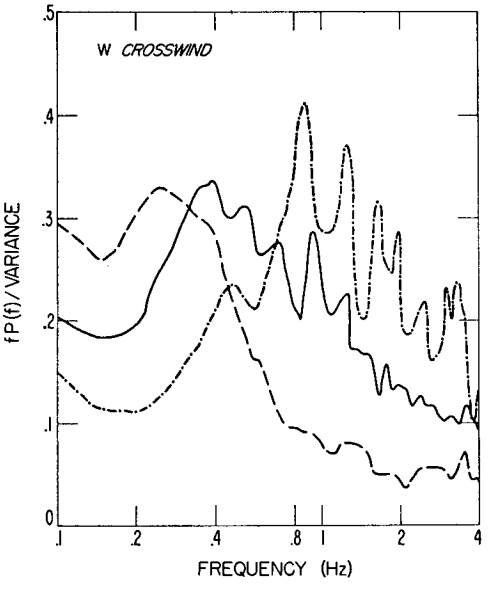

FIG. 4. Same as Fig. 3 except for three crosswind flights.

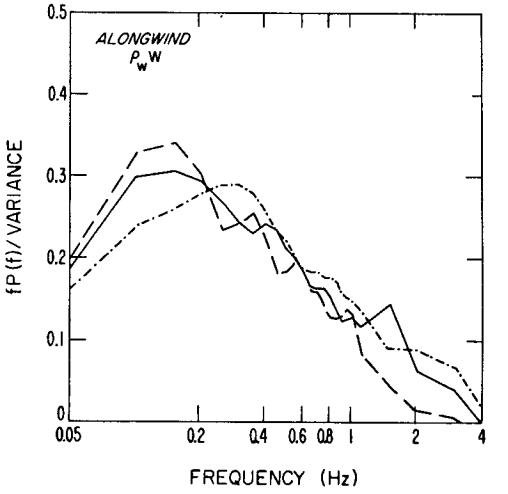

FIG. 5. Composite of all alongwind water vapor flux spectra taken near FLIP during BOMEX at 152 m ($n=11$, dashed line), 45 m ($n=14$, solid line), and 18 m ($n=11$, dash-dotted line). The frequency-weighted spectral density is normalized by the average variance of all the samples, n is the sample size, and the 90% confidence limits are very close to the curves presented.

constructed for $\rho_w'w'$ at each altitude and heading (Figs. 5 and 6). This presentation demonstrates very clearly the tendency for the peak variance to move to lower frequencies with increasing height, i.e., the large eddies are more effective in transporting humidity with increasing height while the small eddies contribute more to the flux of water vapor near the sea surface. As before, the crosswind composite shows the trends more definitely than the alongwind composite, allowing us to plot the wavelength of the maximum spectral density vs height (Fig. 7).

Each data point for Fig. 7 is the average of more than 10 crosswind flights. The relationship appears to be linear on a log-log plot with a 10 m height yielding a wavelength intercept of $\sim$100 m and a slope of 0.7.

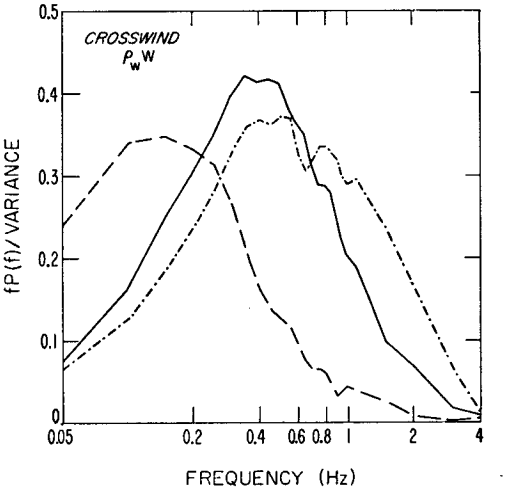

FIG. 6. Same as Fig. 5 except for all crosswind water vapor flux spectra taken near FLIP.

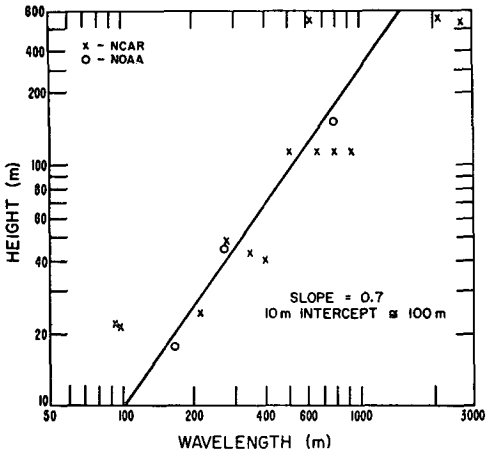

FIG. 7. Variation of wavelength of maximum spectral density vs altitude. Data were taken from Fig. 6 with the crosses denoting NCAR data used for comparison.

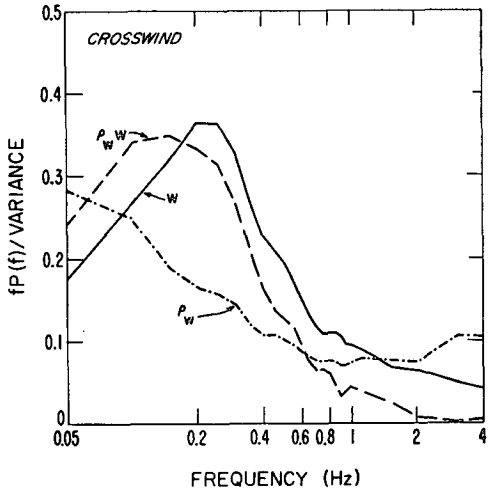

FIG. 9. Same as Fig. 8 except for crosswind spectra.

We have the opportunity to compare our results with similar data taken from an analysis of $\rho_w'w'$ spectra obtained from crosswind measurements taken onboard the National Center for Atmospheric Research Queen Air (Donelan, 1970). The 10 m intercept and slope computed from a least-squares fit to the NCAR data are, respectively, 85 m and 0.7. Since the NCAR instrumentation package was basically different from the RFF package, we conclude that the increase of the wavelength of maximum spectral density with height is a well-defined basic phenomenon occurring in the BOMEX area.

If the components of E are examined as in Figs. 8 and 9, a strong low-frequency trend is seen in the ρ_w' spectra with a definite maximum in w' which appears to be reflected in the spectrum of $\rho_w'w'$ (Fig. 9).

If we look ahead to data taken in long level flights across the BOMEX array at 152 m and 30 m (Fig. 12), the crosswind spectra of $E_{10}{}^{10}$ again show the trend of a spectral peak at lower frequencies with increasing height. The alongwind spectral maximum appears relatively constant with elevation. Table 3 summarizes these results.

We thus conclude that the transport process seems quite different when viewed alongwind than it does when viewed crosswind whether sampled at a fixed location such as FLIP or at intervals across the array. This reveals to us an extraordinary organization of the clear air convection regime in the lower subcloud layer. This observation may be helpful in interpreting data taken from fixed platforms, such as FLIP, which would be representative of alongwind data. There will be further discussion of this point in Section 8.

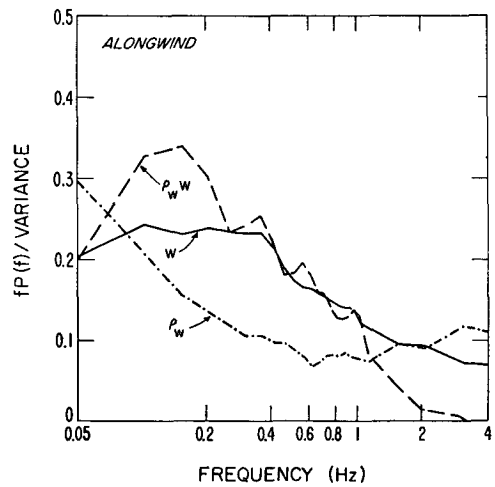

FIG. 8. Composite of 11 frequency-weighted spectral densities for $\rho_w'w'$, ρ_w', and w' taken alongwind at 152 m. The normalizing variance is the average variance of the 11 runs used.

5. Influence of aircraft vertical excursions: Phugoid motion

The extreme, and anomalous, low-frequency trend in the ρ_w' spectra of the 5-min samples was investigated by examining the ρ_w' spectra of the 10-min samples. A composite of all 10-min samples, arranged by altitude and heading (Fig. 10), shows a common frequency of maximum spectral density. Inspection of a more detailed composite reveals this frequency to be 0.024 Hz, irrespective of time, position, heading or altitude. A general formula for the frequency of the phugoid motion of an aircraft (Duncan, 1959) is

$$f_p=\frac{g}{4.44V}, \tag{2}$$

TABLE 3. Frequency (Hz) of spectral maxima for 10-min samples of water vapor flux $E_{10}{}^{10}$. Wavelength is in parentheses.

Altitude	Crosswind	Alongwind
33 m	~0.4 (230 m)	~0.05 (1860 m)
152 m	0.08–0.2 (1160–460 m)	~0.05 (1860 m)

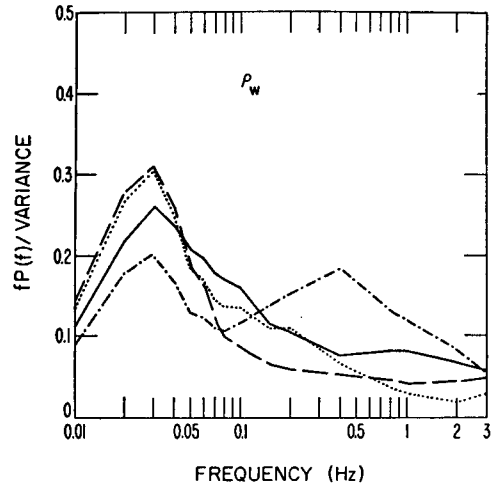

FIG. 10. Composite of all water vapor density spectra taken from 10-min sample lengths. The frequency-weighted spectral density is normalized to the average of all water vapor density variances used in a particular composite. There were approximately four runs at each altitude and heading. Alongwind spectra: 152 m (long dashes) and 33 m (solid line); crosswind spectra: 152 m (dash-dotted line) and 33 m (dots).

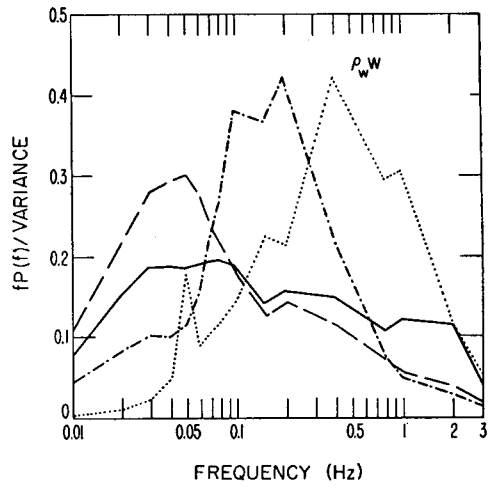

FIG. 12. Same as Fig. 10 except for water vapor flux spectra.

where V is the aircraft true airspeed in MKS units. The phugoid frequency, calculated for 93 m sec^{-1}, the mean true airspeed of the RFF aircraft for the 10-min runs, is 0.0237 Hz or a wavelength of 3.9 km. The w' spectra do not reflect the phugoid motion (Fig. 11), since utilization of the inertial platform information is able to remove aircraft-induced vertical motions. Although this motion may be contributing to the form of the ρ_w' spectra, its effects seem minimized by that of w' in the final $E_{10}{}^{10}$ spectra (Fig. 12).

6. Frequency distributions of w' and ϱ_w'

Cumulative frequency distributions of ρ_w' and w' at 18 m derived from six runs made near FLIP on 11 May

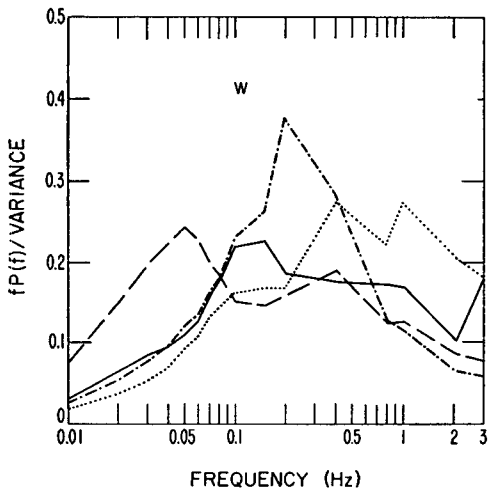

FIG. 11. Same as Fig. 10 except for vertical velocity spectra.

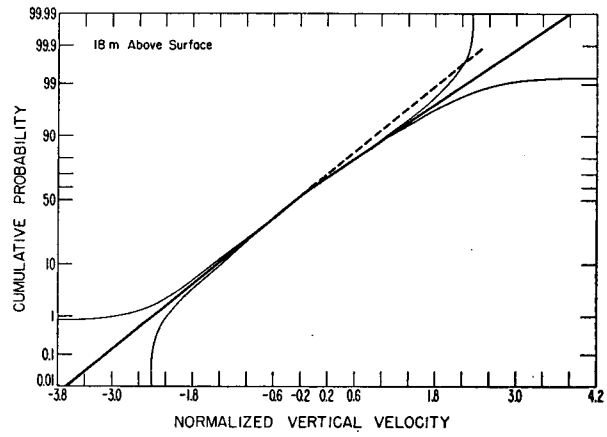

a.

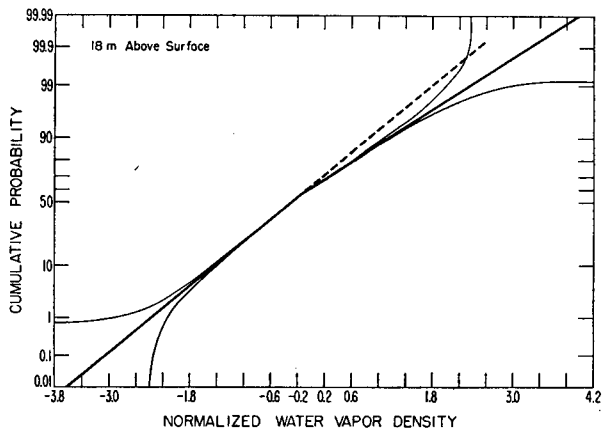

b.

FIG. 13. Cumulative frequency distributions of w', a., and ρ_w', b., for six runs at 18 m flown on 11 May 1969 near FLIP. Data were normalized to their respective variances. There were 6000 points in each sample. The 99% confidence intervals enclose the straight line approximation to the distribution. The dashed line is an extension of the lower straight line approximation.

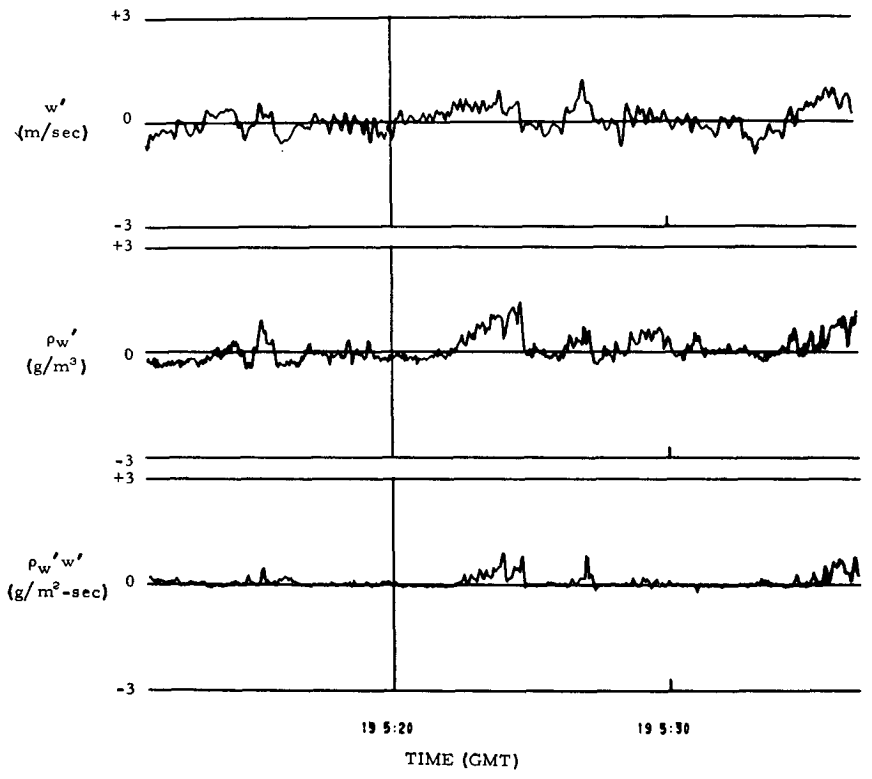

FIG. 14. Sample of time series of w', ρ_w' and $\rho_w'w'$ taken on an 18 m run upwind on 11May 1969 during BOMEX. Data were taken at 20 samples sec^{-1}.

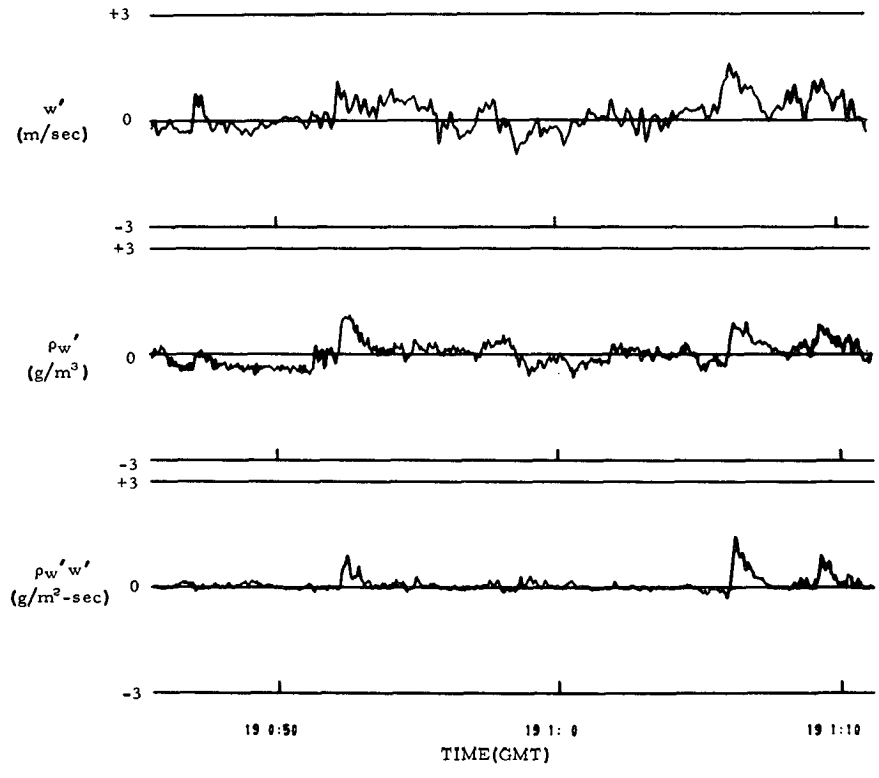

FIG. 15. Same as Fig. 14 except for downwind at 46 m.

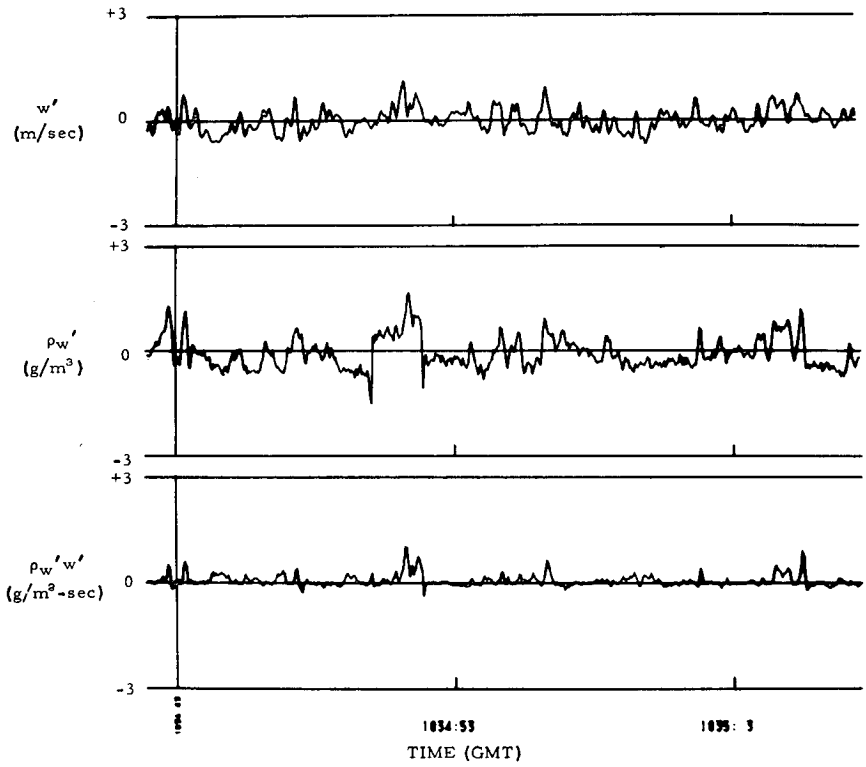

FIG. 16. Same as Fig. 14 except for crosswind at 18 m.

1969 are shown in Fig. 13. The data were normalized by their standard deviations. While the scatter of points at the "tails" of the distribution are typical of cumulative frequency distributions constructed from a finite sample of data, the scatter is very slight for the portions of the distributions between 5 and 95%. A plot of the frequency distribution reveals a monomodal distribution which is slightly skewed positive. It is this type of frequency distribution which is well approximated by a log normal density function (Brooks and Caruthers, 1953). The central portion of the cumulative distribution is approximated by two straight lines whose slopes are significantly different, implying the existence of a bimodal frequency distribution instead of a monomodal one. We take the lower slope (smaller relative variance) to be indicative of the slowly subsiding trade wind environment and the upper slope (higher relative variance) to be indicative of the upward moving convective elements which we feel are transporting a major portion of water vapor from the sea surface into the upper subcloud layer. Similar dual-sloped cumulative frequency distributions of vertical velocity, temperature and refractive index have been found for unstable conditions over land (Frisch, 1970; Lenschow, 1970; Wickerts, 1970). We therefore suggest that the time series should contain the signatures of *at least* two distinct phenomena.

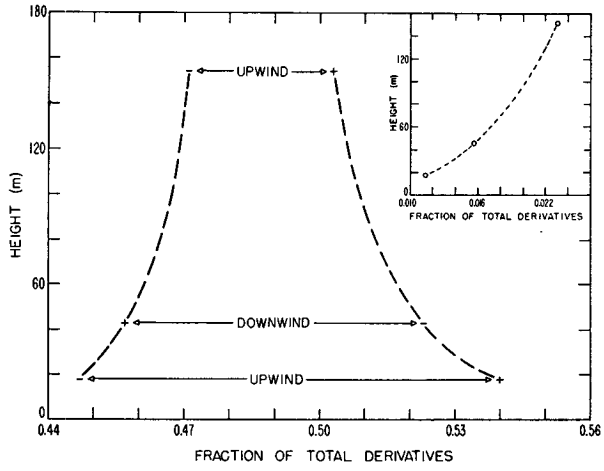

FIG. 17. Fractions of total number of time derivatives of ρ_w which are positive (+) and negative (−) vs height. Heading of aircraft is indicated between arrows. Each value is an average of data taken from three runs. Insert is fraction of derivatives equal to zero vs height.

7. Time series signatures

Examples of typical time series for upwind, downwind and crosswind flights are shown in Figs. 14–16, respectively. A comparison of the alongwind and crosswind ρ_w' traces shows a striking difference between them. The alongwind traces appear to have a ramp-like character while the crosswind traces have a "top hat" signature. Further, the ramp signature reverses in

going from an upwind to a downwind flight. The flux is intermittent in character and the higher values of instantaneous flux are those variations in ρ_w' which are not independent of w.

Quantitative evidence of the ramp character of the alongwind traces is presented as average variations of $\partial\rho_w'/\partial t$ with heading and altitude for all the flights made on 11 May 1969 (Fig. 17). The model of a convective element we propose is one which is spatially oriented with a sharp decrease of ρ_w' to windward of the maximum and a slow decrease of ρ_w' to leeward of the maximum (see Fig. 15). This model predicts a higher frequency of positive than negative derivatives of ρ_w' when flying upwind. This signature should reverse on downwind flights with the frequencies of negative derivatives exceeding positive derivatives. When viewed against a variation in altitude, the difference in frequency of positive and negative derivatives should decrease, if the convective element is losing identity due to entrainment and detrainment. Fig. 17 follows the proposed model.

This particular time series signature allows us to speculate on possible mechanisms which may transport a major portion of water vapor flux in the BOMEX area. The variability of the cross and downwind spectra plus the behavior of the individual traces suggests that a combination of horizontal roll vortices (Faller, 1965; Faller and Kaylor, 1966; Hanna, 1969; Kuettner, 1959; Brown, 1970) and either convective plumes or puffs under a shear flow condition (Scorer, 1958, 1959; Hall, 1962; Richards, 1968; Lilly, 1971) is operative. It seems evident from the flux spectra that the frequency of maximum spectral density is smaller on alongwind runs than on crosswind runs. This phenomena has recently been observed over the Colorado high plains in unstable conditions (Lenschow, 1970). The observation leaves one in doubt as to whether this is characteristic of a horizontal roll vortex system or a convective element or both. The individual time series traces display signatures indicative of the plume or puff under shear.

Critical tests to differentiate between these various models which may act in the oceanic boundary layer are the subjects of the authors' continuing research.

8. Concerning the sampling problem

The results given above represent one end product of a very extended and complex experiment. Many decisions had to be made as we went along. Our chief guide during the flights, for example, was the refractometer output. Similar decisions were made regarding the choice of filters, sampling rate and averaging time. For example, data in Figs. 14–16 indicate 50–100 bursts of instantaneous flux on alongwind runs compared to several hundred bursts on crosswind runs. As a result of such considerations, it was obvious that alongwind runs differed significantly in character from crosswind runs; however, low-frequency differences were not at all apparent. We now reexamine our decisions regarding filters, sampling rate and averaging time in the light of the previous discussion.

TABLE 4. Position (Hz) of maximum in the spectrum of water vapor flux.*

	Ht (m)	5-min composites	10-min composites
Alongwind	18	0.25–0.35 (5)	—
	30	—	0.025–0.1 (12)
	45	0.07–0.2 (5)	—
	152	0.07–0.2 (5)	0.025–0.05 (12)
Crosswind	18	0.3–0.5 (6)	—
	30	—	0.4 (12)
	45	0.3–0.5 (6)	—
	152	0.07–0.3 (6)	0.09–0.2 (12)

* Figure number is given in parentheses.

Ideally one wishes to have a well-defined spectrum with a pronounced peak and zero variance at the frequency extremes. This, of course, is not the case for the flux spectra. If one examines the along- and crosswind spectra, one concludes that the best defined are from the 18 and 45 m crosswind runs. Further, if the 10-min samples are reexamined for regions of peak contribution to the covariance (see Table 4), there is notably more contribution to the covariance at significantly lower frequencies for 10-min alongwind runs than for similar 5-min runs. This is not the case for the crosswind samples. For these reasons we consider the most reliable data are those from the crosswind runs at 18 and 45 m. This conclusion implies that a fixed site measurement would require very long runs to obtain similar values, since it measures the alongwind structure. For example, to reproduce the same amount of air sampled by the 10-min runs at a fixed site, one would require 200-min records for a 5 m sec^{-1} wind. This could well be offset by the relative importance of smaller scales as indicated in Fig. 7, provided that the transport process is horizontally homogeneous at these lower heights.

9. Summary

We have presented several observations and conclusions from water vapor flux measurements taken during BOMEX which can be summarized as follows. The variation of water vapor flux is small in the interval 18 to 152 m in the lower subcloud layer which implies a constant flux layer for water vapor. Water vapor flux appears to vary appreciably on a time scale within a day, on a day-to-day scale and on a spatial basis. The average value of water vapor flux for the RFF DC-6 missions during the first three phases of BOMEX is approximately 0.5 cm day^{-1}. Variation of the shape of the spectra of $\rho_w'w'$ shows the maximum variance to march to lower frequencies as the measurement height is increased. Comparison of the power-law approxima-

tion of this spectral variation with height with independent measurements shows very close agreement. Compromise of the ρ_w data by the aircraft phugoid motion is clearly demonstrated; however, the water vapor flux values are only slightly affected by this error. We conclude that the process controlling the transport of water vapor appears to show significant differences when crosswind flights are compared to alongwind flights, implying an organization of water vapor transport in the lower subcloud layer.

Acknowledgments. The authors thank Dr. O. Lappe for his calibration of the inertial platform and Mr. L. Rinaldi for careful preparation of the data for analysis.

The original flight plans and data reduction specifications were arrived at by the present authors and the late Dr. Ben Davidson.

We also express our appreciation of many discussions with Dr. Joshua Holland, plus his careful review of the manuscript.

R. L. Grossman gratefully acknowledges discussions with Dr. Y. Hsueh regarding certain aspects of the time series.

APPENDIX A

Error Analysis

This discussion will present an analysis of instrumental errors in the individual values of $\rho_w'w'$. The average flux of water vapor, assuming a zero mean value for w and ρ_w, is determined by

$$\mathrm{Cov}(\rho_w'w')=\frac{1}{\tau}\int_0^\tau \rho_w(\tau)w(\tau)d\tau=\overline{\rho_w'w'}. \quad \text{(A1)}$$

If we consider the measured value, $\hat{\rho}_w'$ for example, to be made up of a true value, ρ_w', and some random error, $\epsilon(\rho_w')$, then

$$\hat{\rho}_w'=\rho_w'+\epsilon(\rho_w'). \quad \text{(A2)}$$

When ρ_w is determined from the radio refractive index, we have

$$\rho_w=f(N,T,P), \quad \text{(A3)}$$

where N is the refractive index, T the absolute temperature, and P the static pressure, so that $\epsilon(\rho_w')$ can be considered as the root-sum-square of the errors which are inherent in the instruments measuring N, T and P, i.e.,

$$\epsilon(\rho_w')=(d\rho_w'^2)^{\frac{1}{2}}$$

$$=\left[\left(\frac{\partial\rho_w}{\partial N}dN\right)^2+\left(\frac{\partial\rho_w}{\partial T}dT\right)^2+\left(\frac{\partial\rho_w}{\partial P}dP\right)^2\right]^{\frac{1}{2}}. \quad \text{(A4)}$$

Within the brackets the partial derivative is determined from the functional form given in (A3) and the differentials are experimentally determined from the resolution characteristics of the instruments. In the calculation of the numerical value of the partial derivative certain mean values of N, T and P must be obtained from actual flight conditions or assumed as indicative of average conditions during the experiment.

From the above considerations and the values given in Appendix B, we calculated the resolution accuracy of ρ_w' to be 1.068×10^{-8} gm m^{-3} and the corresponding resolution of w' as 5.8 cm sec^{-1}.

Combining (A1) and (A2), while extending the definition given in (A2) to $\hat{w}'$, we can write for the flux of water vapor,

$$\overline{\hat{\rho}_w'\hat{w}'}=\overline{[\rho_w'+\epsilon(\rho_w')][w'+\epsilon(w')]}$$
$$=\overline{\rho_w'w'}+\overline{\epsilon(\rho_w')w'}+\overline{\epsilon(w')\rho_w'},$$
$$+\overline{\epsilon(\rho_w')\epsilon(w')}. \quad \text{(A5)}$$

If all measurements are independent of one another, then a normal and reasonable assumption is that no correlation exists between the quantities given the last three terms on the right-hand side so that (A5) becomes

$$\overline{\hat{\rho}_w'\hat{w}'}=\overline{\rho_w'w'}. \quad \text{(A6)}$$

Thus, the accuracy of the measurement is dependent only upon sampling rate and averaging time, factors not considered in this analysis of errors.

However, in our particular analysis we cannot consider all measurements as independent. For instance,

$$w'=f(T,\ P,\ \text{and other terms}), \quad \text{(A7)}$$

so that when comparing with (A3) we see absolute temperature and static pressure are common to both w' and ρ_w'. Therefore, we consider

$$\left.\begin{aligned}\epsilon(\rho_w')&=a\epsilon_T+b\epsilon_P\\ \epsilon(w')&=c\epsilon_T+d\epsilon_P\end{aligned}\right\}. \quad \text{(A8)}$$

Substituting the set of equations (A8) into (A5), and since the true value is independent of error,

$$\overline{\hat{\rho}_w'\hat{w}'}=\overline{\rho_w'w'}+\overline{(a\epsilon_T+b\epsilon_P)(c\epsilon_T+d\epsilon_P)}. \quad \text{(A9)}$$

Expanding the second term in (A9), we obtain

$$\epsilon(\overline{\rho_w'w'})=ac\overline{\epsilon_T\epsilon_T}+(ad+bc)\overline{\epsilon_P\epsilon_T}+bd\overline{\epsilon_P\epsilon_P}. \quad \text{(A10)}$$

Since P and T are independent instruments, we assume that

$$\overline{\epsilon_P\epsilon_T}=0,$$

and (A10) reduces to

$$\epsilon(\overline{\rho_w'w'})=ac\epsilon_T^2+bd\epsilon_P^2. \quad \text{(A11)}$$

Eq. (A9) then becomes

$$\overline{\hat{\rho}_w'\hat{w}'}=\overline{\rho_w'w'}+ac\epsilon_T^2+bd\epsilon_P^2. \quad \text{(A12)}$$

The latter two terms on the right-hand side of (A12) sum to a value of 0.00234 gm^{-2} sec^{-1} or 0.02 cm day^{-1}. This value, the instrumental error in the water vapor flux measurement, is approximately 4% of a typical value of water vapor flux obtained during BOMEX.

APPENDIX B

Resolution Errors of Parameters used to Calculate w' Error

Parameter	Value (in appropriate units)
mean normal acceleration of aircraft (maximum value)	294 cm sec^{-1}
mean pitch angle of aircraft	0.87 rad (maximum value)
resolution of temperature	0.05K (courtesy R. E. McGavin, NOAA)
resolution of impact pressure	10^{-4} mb, differential
resolution of static pressure	16×10^{-4} mb
resolution of pitch angle	5×10^{-4} rad
resolution of normal acceleration	2.94 cm sec^{-2}
resolution of longitudinal acceleration	0.980 cm sec^{-2}
resolution of vertical sensing vane angle of attack	3.49×10^{-4} rad
resolution of aircraft roll angle	5.235×10^{-4} rad
mean true air speed	9500 cm sec^{-1}
resolution of lateral sensing vane angle of attack	3.49×10^{-4} rad
resolution of pitch angle rate	3.49×10^{-4} rad sec^{-1}

REFERENCES

Brooks, C. E. P, and N. Caruthers, 1953: *Handbook of Statistical Methods in Meteorology*. London, H. M. Stationary Office, 412 pp.

Brown, R. A., 1970: A secondary flow model for the planetary boundary layer. Sci. Rept., Dept. of Atmospheric Sciences, University of Washington, 67 pp.

Crooks, W. M., *et al.*, 1968: Project HICAT high altitude clear air turbulence measurements and meteorological correlations. Tech. Rept. AFFDL-TR-68-127, Vol. 1, Air Force Flight Dynamics Lab., 308 pp.

Donelan, M., 1970: An airborne investigation of the structure of the atmospheric boundary layer over the tropical ocean. Ph.D. dissertation, Dept. of Physics, University of British Columbia, 146 pp.

Duncan, W. J., 1959: *The Principles of the Control and Stability of Aircraft*. Cambridge University Press, 391 pp.

Faller, A. J., 1965: Large eddies in the atmospheric boundary layer and their possible role in the formation of cloud rows. *J. Atmos. Sci.*, **22**, 176–184.

——, and R. Kaylor, 1966: A numerical study of the instability of the laminar Ekman layer. *J. Atmos. Sci.*, **23**, 466–480.

Friedmann, H., *et al.*, 1970: ESSA Research Flight Facility aircraft participation in BOMEX. *Bull. Amer. Meteor. Soc.*, **51**, 822–834.

Frisch, A. S., 1970: A study of convective elements in the atmospheric boundary layer. Ph.D. dissertation, Dept. of Geophysics, University of Washington, 95 pp.

Hall, J., 1962: The rise of an isolated thermal in wind shear. *Quart. J. Roy. Meteor. Soc.*, **88**, 394–411.

Hanna, S. R., 1969: The formation of longitudinal sand dunes by large helical eddies in the atmosphere. *J. Appl. Meteor.*, **8**, 874–883.

Holland, J., 1970: Preliminary report on the BOMEX sea-air interaction program. *Bull. Amer. Meteor. Soc.*, **51**, 809–819.

Kuettner, J., 1959: The band structure of the atmosphere. *Tellus*, **11**, 267–294.

Lenschow, D. H., 1970: Airplane measurements of planetary boundary layer structure. *J. Appl. Meteor.*, **9**, 874–884.

Lilly, D. K., 1971: Comments on "Case studies of a convective plume and a dust devil". *J. Appl. Meteor.*, **10**, 590–591.

McGavin, R. E., and M. J. Vetter, 1963: Radio refractometry and its potential for humidity studies. *Humidity and Moisture: Measurement and Control in Science and Industry*, Vol. 2, New York, Reinhold, 553–560 pp.

Richards, J. M., 1968: Inclined buoyant puff. *J. Fluid Mech.*, **22**, 681–692.

Rinaldi, L., 1970: BOMEX vapor flux study: Data processing procedure. Progress Rept. to NOAA, Wave Propagation Laboratory, Contract E22-93-70(N), 19 pp.

Scorer, R. S., 1958: *Natural Aerodynamics*. New York, Pergamon Press, 312 pp.

——, 1959: The behavior of chimney plumes. *Intern. J. Air Pollution*, **1**, 198–220.

Wickerts, S., 1970: The refractive index field in the lowest 2000 m of the atmosphere. Research Institute of National Defense (Sweden), *FOA Repts.*, **4**, No. 3, 1–16.